The Journal of Chemical Physics

The ionic and ground states of gamma-pyrone. The photoionization spectrum studied by synchrotron radiation and interpreted by configuration interaction and density functional calculations

Cite as: J. Chem. Phys. **158**, 014304 (2023); https://doi.org/10.1063/5.0128764
Submitted: 30 September 2022 • Accepted: 13 December 2022 • Accepted Manuscript Online: 13 December 2022 • Published Online: 03 January 2023

Michael H. Palmer, Marcello Coreno, Monica de Simone, et al.

The Journal of Chemical Physics ARTICLE scitation.org/journal/jcp

The ionic and ground states of gamma-pyrone. The photoionization spectrum studied by synchrotron radiation and interpreted by configuration interaction and density functional calculations

Cite as: J. Chem. Phys. 158, 014304 (2023); doi: 10.1063/5.0128764
Submitted: 30 September 2022 • Accepted: 13 December 2022 •
Published Online: 3 January 2023

Michael H. Palmer,[1,a] Marcello Coreno,[2,b] Monica de Simone,[3,b] Cesare Grazioli,[3,b] Nykola C. Jones,[4,b] Søren Vrønning Hoffmann,[4,b] R. Alan Aitken,[5,b] and Dheirya K. Sonecha[5,b]

AFFILIATIONS

[1] School of Chemistry, University of Edinburgh, Joseph Black Building, David Brewster Road, Edinburgh EH9 3FJ, Scotland, United Kingdom
[2] ISM-CNR, Instituto di Struttura della Materia, LD2 Unit, 34149 Trieste, Italy
[3] IOM-CNR, Istituto Officina dei Materiali, Basovizza SS-14, Km 163.5, 34149 Trieste, Italy
[4] ISA, Department of Physics and Astronomy, Aarhus University, Ny Munkegade 120, DK, 8000 Aarhus C, Denmark
[5] School of Chemistry, University of St. Andrews, North Haugh, St. Andrews, Fife, KY16 9ST, Scotland, United Kingdom

[a] **Email:** m.h.palmer@ed.ac.uk
[b] **Authors to whom correspondence should be addressed:** marcello.coreno@elettra.eu; desimone@iom.cnr.it; grazioli@iom.cnr.it; nykj@phys.au.dk; vronning@phys.au.dk; raa@st-andrews.ac.uk; and dks1@st-andrews.ac.uk

ABSTRACT

A synchrotron-based photoionization spectrum up to 27 eV represents a considerable improvement in resolution over early He(I) and He(II) spectra. Symmetry-adapted coupled cluster calculations of the ionic state sequence give the sequence of state vertical ionization energies (VIE) as $1^2B_2 < 1^2B_1 < 1^2A_2 < 2^2B_1 < 1^2A_1$. Generally, these symmetry-adapted cluster configuration interactions VIE match reasonably well with the experimental spectrum over this wide energy range. Density functional calculations of the corresponding adiabatic terms (AIE) were also performed. Higher energy ionic states were determined by complete active space self-consistent field methods; these include all π-ionizations and some σ-ionic states. These were analyzed by Franck–Condon (FC) procedures and compared with an experiment. The spectral onset is complex, where two states, later shown to be the 1^2B_2 and 1^2B_1 states, are strongly overlapping. The superposition of the FC vibrational structure in the 1^2B_2 and 1^2B_1 states accounts for most of the peaks arising at the onset of the photoelectron spectra. However, the small separation between these two ionic states makes vibronic interaction fairly inevitable. In the absence of Herzberg–Teller analyses for ionic states, we have sought and determined a transition state between the 1^2B_2 and 1^2B_1 states, showing that vibronic coupling does occur. The lack of degradation in the vibrational envelope of the higher of the two states contrasts with our previous work on the halogenobenzenes, where overlapping state envelopes led to considerable widening of the line width at half-height of the higher energy states.

I. INTRODUCTION

Recently, we have reported synchrotron-based, vacuum ultraviolet (VUV) absorption and high-resolution photoelectron spectra (PES) spectra for several highly conjugated molecules, including cyclooctatetraene (COT),[1,2] cycloheptatriene (CHT),[3,4] norbornadiene (NBD),[5,6] and azulene.[7,8] A major difference from preceding work for these high-profile molecules is that we have offered Franck–Condon (FC) and Herzberg–Teller (HT) interpretations of the vibrational structure observed in their VUV spectra and FC for their PES. The use of HT methods for the analysis of PES has not been possible in these studies due to limitations arising from the software available to us, as discussed below. We now report similar studies of the PES of another fully conjugated molecule, γ-pyrone (**1**, shown in Fig. 1). This substance is systematically described as 4H-pyran-4-one. A parallel study of the VUV spectrum will be presented in a later paper. The γ-pyrone PES, under He(I) and He(II) conditions was previously reported,[9] for the valence shell, and for the core C_{1s} and O_{1s} electrons (using AlKα + MgKα). The PES were obtained under the low-resolution conditions of that time (1980), so that vibrational analysis was primitive;[9] indeed, the accompanying theoretical studies,[9] both semi-empirical and *ab initio* using a minimal basis set, were regarded as sufficiently unreliable that the spectral assignments were based on comparisons of ionization energies (IE) with those of related compounds. Our analysis of the higher-resolution PES is accompanied by sophisticated calculations of the electronic structure of the parent molecule and its ionic states.

The properties of γ-pyrone are unusual, especially in terms of reactivity,[10] where it does not behave as a (double) α,β-unsaturated ketone. For example, prolonged treatment with D_2O leads to the 3,5-d_2 isotopomer, while related treatment with ^{18}O-enriched water incorporates ^{18}O at both O-atoms. These changes appear to occur in the pyrone system[11,12] via sequential addition, ring opening, closing, and elimination changes. Both ^1H and ^{13}C nuclear magnetic resonance spectra (NMR) have been studied in considerable detail, including long-range (i.e., across the ring) coupling constants. The interpretation of these values has been controversial since the comparisons with related five- and six-membered ring molecules lead to differing conclusions.[13] The chemical shifts, when compared to those of dihydro-derivatives where the full conjugation is missing, led to the proposition that γ-pyrone supports a ring current.[10,13–16] The C_{2V} structure clearly shows a fully conjugated π-electron system; the initial conclusion that it is an aromatic molecule emerged by consideration of several contributing canonical forms, such as 1B in Fig. 1.

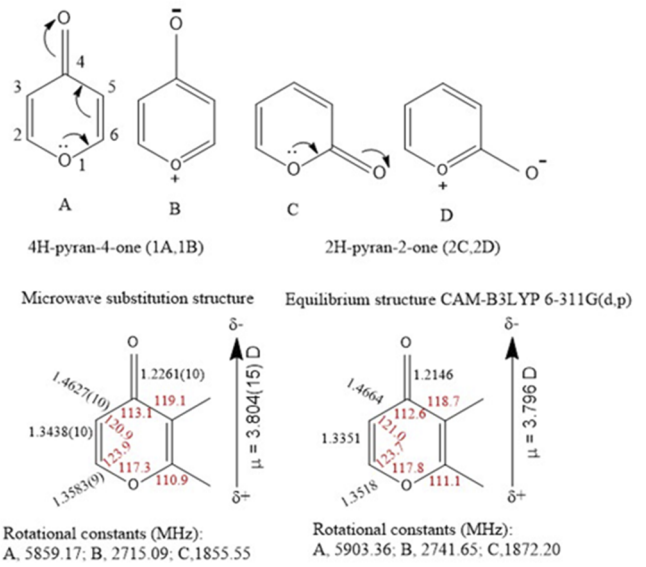

FIG. 1. Top: The structures of the pyran-2- and -4-ones, and the important canonical forms to express the non-classical reactivity. Bottom: A comparison of the microwave substitution structure with the equilibrium structure of γ-pyrone at the CAM-B3LYP level.

However, microwave (MW) substitution structures for γ-pyrone and the three related molecules where one or both O-atoms are replaced by S-atoms, gave complete structures, which showed classical C=C bond lengths and angles.[17–21] The MW structure for γ-pyrone is compared to our equilibrium structure using a standard triple-zeta basis, in Fig. 1, and discussed below. The vibrationally averaged nematic phase γ-pyrone structures determined from ^1H and ^{13}C NMR spectroscopy are in close agreement with the MW results.[22,23] The magnetic susceptibility anisotropies, also analyzed by MW, in terms of local and nonlocal contributions, show that both γ-pyrone and the related lactone (α-pyrone), shown as 2C and 2D in Fig. 1, have negligibly small non-local contributions; thus, both are considered to be non-aromatic by this magnetic criterion.[17,18,21] Earlier discussions in terms of a ring current, based on NMR chemical shifts, then appear to be improbable.[24,25]

II. METHODS

The γ-pyrone sample, CAS registry number 108-97-4, was synthesized by standard methods,[26,27] and the purity checked by ^1H and ^{13}C nuclear magnetic resonance.[11,14]

A. The photoelectron spectrum

This was obtained on the gas-phase line of the Elettra synchrotron (Trieste, Italy), at room temperature, using methods described previously.[1,3] The sample vapor was irradiated with both 30 and 90 eV photon energies. The 30 eV spectrum covers the energy range 8.956–11.756 eV with 1463 data points (DPs), separated by 0.002 eV (16 cm^{-1}). A wider scan using 98 eV photons contains 1972 DPs with a separation of 0.01 eV up to 16.1 eV and 0.025 eV for the range 16.1–45.883 eV. The PES spectrum acquired at hν = 98 eV in the wide range up to 27 eV is shown in Fig. 2 and discussed below in light of our calculated spectral lines.

We adopt a conventional definition of resolution as the minimum separation between two spectral lines where it is possible to distinguish between them; thus, the 30 eV spectrum corresponds to an overall resolution close to 8.5 meV. The precision of the measured energies and the resolution were also determined from the half-width of argon PES lines, which are known from the literature; Argon was added to the sample as an additional calibrant. Additional peak-fit statistics, using the Multi-peak Fit (Version 2.22) program, including the absolute positions of the principal PES peaks, are listed in the supplementary material as Table SMI. The complex onset of

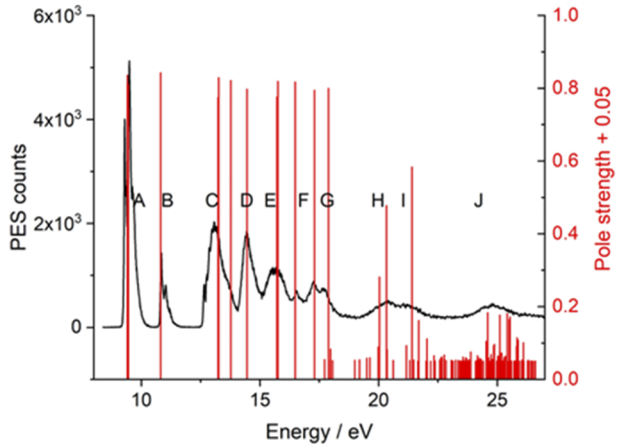

FIG. 2. The wide scan photoelectron spectrum from 8 to 27 eV acquired at hν = 98 eV; the energy resolution is circa 40 meV. The principal bands are labeled A–J. The vertical bars are the pole strengths (intensities) from the symmetry-adapted cluster configuration interaction (SAC-CI) calculations of the ionic state energies. The pole strengths have been increased by 0.05 units to make the numerous very weak states more obvious.

the PES in the range 9.2–10 eV was analyzed, as shown in Figs. 3(a) and 3(b), and is discussed below.

B. Theoretical methods

Several computational chemistry suites were used since none offered us a complete analysis. The equilibrium structures for the X^1A_1 ground state and several of the lowest ionic states of each symmetry were determined using the GAUSSIAN suite (G-16).[28] Several density functional theory (DFT) functionals[29–31] were tested. Overall, the long-range corrected, Coulomb-attenuating version of the Becke method with the Lee–Yang–Parr hybrid functional (CAM-B3LYP)[31,32] gave the best results. This conclusion is based on energy separations between ionic states and also the balance between the 0-0 band and vibrational satellite intensities determined by the Pisa software, as discussed below.

The 2^2B_1 and 3^2B_1 states are not accessible by that procedure since the collapse to the 1^2B_1 state occurs during structure determination; these and other higher states were successfully accessed by complete active space SCF (CASSCF). The number of roots of the required symmetry is selected, and the structure is optimized for that root (here 1, 2, or 3). Initially, the Hartree–Fock wave-function is reordered to make the active CASSCF molecular orbitals (MOs) the highest occupied orbitals; for example, $1b_1^2$, $2b_1^2$, and 3^2b_1; the active virtual orbitals were similarly re-ordered to be of the required symmetry. In this way, the CASSCF method is forced to generate the required states of appropriate symmetry. Using the 6-311G(d, p) basis set, a 3- (or 5-) electron within the 8-orbital CASSCF, conventionally termed CAS[3,8]SCF, gave two roots of $^2B_1$ symmetry as linear combinations; the higher energy one was optimized. The same procedure was applied to the CAS[5,8]SCF case, leading to the third state. A perusal of the leading configurations showed that the state required was present and that no higher intruder state had been obtained. Similar CASSCF procedures were performed for both

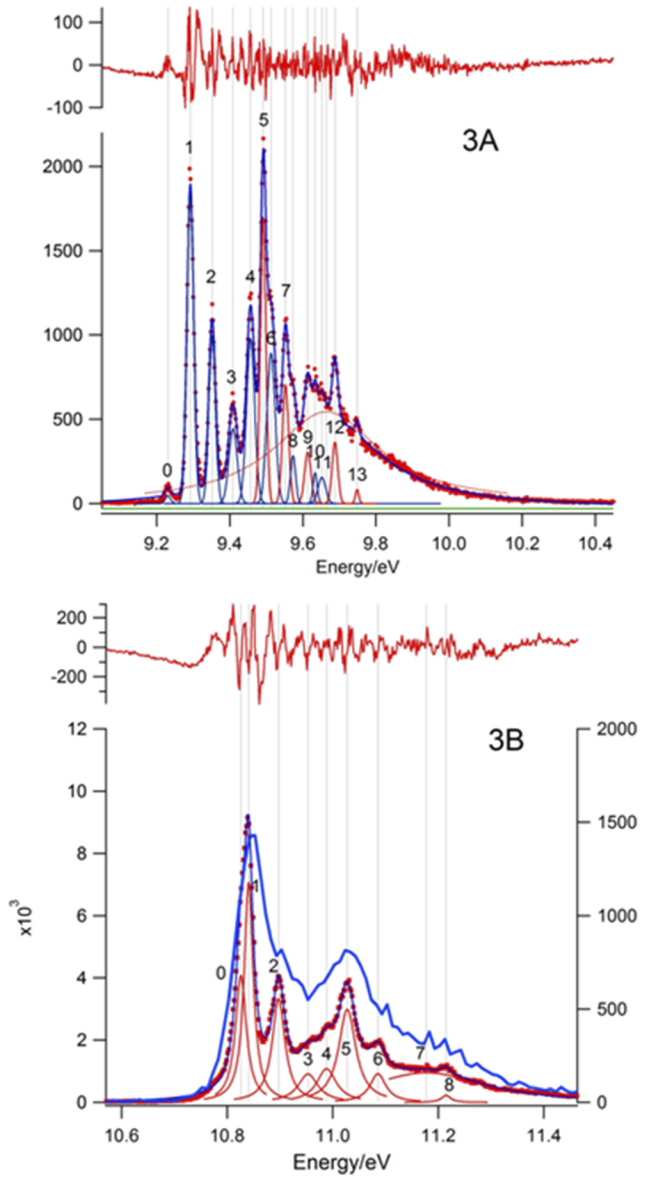

FIG. 3. The onset (3A) and second band (3B) of the γ-pyrone PES measured at hν = 30 eV, energy resolution circa 9 meV. Both are discussed in detail below. The higher resolution spectrum of the second band is compared to the lower resolution measurements performed at hν = 98 eV (blue line in the figure). The measured peak positions are shown in the supplementary material as Table SM1.

the 2 and 3^2B_2 states, but we were unable to obtain an equilibrium structure for the 2^2A_1 state.

Input wave-functions for the Franck–Condon (FC) analyses[33–35] were determined by the CAM-B3LYP or CASSCF methods. Adiabatic terms (AIE) determined by these methods in G-16 are based upon energy differences between the ground and excited states, *both at the excited state equilibrium geometry*; standard AIE in spectroscopy use the difference in energy between

the excited state and the ground state, *each at their equilibrium structures*. Potentially, these differences could alter the state symmetry sequence of ionic states when closely spaced states occur. Direct calculation of the vertical ionization energies (VIE) was also performed by the symmetry-adapted cluster configuration interaction (SAC-CI)[36–40] method within G-16. These were determined by the equilibrium structure of the X^1A_1 ground state. The reference configurations were from the singles and doubles configuration interaction levels (RefCISD). The active space for the SAC-CI included orbital energies from −1.1 to 0.86 a.u.

We also used the Tamm–Dancoff approximation (TDA) method[41–43] over a wider energy range; this single excitation CI method, a simpler method, is a component of the GAMESS-UK suite.[44] The 6-311G(d, p) basis set, a valence triple zeta (VTZ) basis,[45–47] was used throughout this study; the core orbitals ($1a_1$ to $5a_1$, $1b_2$ and $2b_2$), representing the $1s_O$ and $1s_C$ orbitals, are frozen. Valence shell labeling of orbitals is used, and these are $1a_1$ to $8a_1$, $1b_1$ to $3b_1$, $1b_2$ to $6b_2$, and $1a_2$; all these are doubly occupied in the X^1A_1 ground state.

It is important to note that G-16, including the Pisa software for FC studies, labels the harmonic frequencies in ascending frequency order irrespective of symmetry, which contrasts with the normal spectroscopic convention: $a_1 < a_2 < b_1 < b_2$. In γ-pyrone, where FC processes are occurring, the vibrationally active modes are all of a_1 symmetry, with labels 1–11.

III. RESULTS AND DISCUSSION

A. The ground state of γ-pyrone

1. The experimental and calculated structures for γ-pyrone

A comparison of the microwave substitution C–C and C–O bond lengths[17,18] with the CAM-B3LYP equilibrium structure, as in Fig. 1, shows median differences (MD) of 0.0065 Å overall; the C=O bond length is larger by 0.0115, Å with the C=C bond lengths being slightly smaller. The absolute MD in the angles (internal CCC and external CCH) is 0.2°. Similarly, a comparison between the MW rotational constants (RC, A, B, and C) and the calculated ones gives differences of −44, −27, and −17 MHz for A, B, and C, respectively. Substitution and equilibrium structures are expected to be very similar but not identical; these very small differences demonstrate the high quality of these calculations. The calculated dipole moment is close to that determined by the Stark effect.[19] The structure shown in Fig. 1 is adopted for the X^1A_1 ground state throughout the FC analyses below. The calculated structures for the ionic states, which are not central to the present paper, are shown in the supplementary material as SM2.

2. The γ-pyrone X^1A_1 vibrational spectrum

Theoretical determination of the vibrational envelopes of the ionic states is important in this study; consideration of the ground state data will give an indication of the reliability of the theoretical results for the ionic states. In addition to gas-phase and theoretical investigations,[48,49] this has previously been investigated by matrix-isolation Fourier-transform infrared spectroscopy (FTIR), where the absorption bands were assigned by Hartree–Fock calculations at the 6-31G* level.[50] Our theoretical CAM-B3LYP study was performed with the larger 6-311G(d,p) basis set, at both the harmonic and anharmonic frequency levels. The anharmonic procedure includes two-order perturbation theory (PT2).[51] The results, shown in Table I, lead to a correlation between the calculated anharmonic frequencies and the experimental Raman or IR data as $\nu_{Anhar} = 0.993(4)^*\nu_R - 1.1(66)$ cm^{-1} and $\nu_{Anhar} = 0.976(5)^*\nu_{IR} + 15(10)$ cm^{-1}, respectively, where the standard errors (SE) are in parentheses. The intercept for the Raman correlation is significantly lower than its SE, which suggests a zero intercept, while the slope is close to unity; similarly, the IR intercept is close to its SE. The correlation coefficients (adjacent R^2) are 0.9996 and 0.9995, respectively. This near identity between the theoretical and experimental ground state frequencies supports Fausto *et al.*[50] and ourselves in assigning the experimental spectra on the basis of correlating two sequences of ascending numbers. We note in passing that Fausto *et al.*[50] suggest that Fermi resonances (FR) occur close to 1412 and 1685 cm^{-1}. The present study identifies several FR, including ones at 1412 and 1422 cm^{-1}, but none near 1685 cm^{-1}. The 1412 cm^{-1} one involves modes 22 and modes 11 + 17.

3. The nature of the bonding in γ-pyrone

The atoms in molecules (AIM) approach, devised by Bader,[52–54] was used to evaluate the variation in electron density along the inter-nuclear distances for the constituent atoms. This is determined directly, for any electronic state, by integration of the *ab initio* wavefunctions. If the electron density along the axis between each pair of atoms, whether directly bonded or not, reaches a minimum value, then a critical point (CP) is defined between that pair of atomic neighbors. The positions of these CP minima define the range of each atomic basin. In the absence of a second nucleus, non-bonded electrons, as for the O-atom lone pairs in γ-pyrone, do not generate a CP in AIM. Similarly, as a result of the planar molecule where the π-electron density is identical above and below the internuclear axes, no CP arises. Thus, the CP are effectively determined by polarization of the σ-electron density. The role of lone pairs and π-bonds has been considered in AIM terms[55] for dissociation processes, but this is irrelevant here since we are discussing the AIM issue at equilibrium.

The CP for the X^1A_1 and lowest ionic (1^2B_2) states, are shown in Fig. 4. Those between the $C_\beta C_\gamma$ bonds, involving atoms $C_3 + C_4$, and $C_4 + C_5$, lie close to the mid-point of these bonds, implying nearly equivalent atomic basins. That is not the case for the $C_\alpha C_\beta$ bonds, C_2C_3 and C_6C_5, where the CP is shifted toward the β-positions. This shows that the bonds are polarized in the sense $C_\alpha^{\delta+}C_\beta^{\delta-}$. All C–O and C=O bonds are strongly polarized $C^{\delta+}O^{\delta-}$, with the (notionally single) C–O σ-bonds being more polar than the C=O π-bond. All C–H bonds are polarized $C^{\delta-}H^{\delta+}$. There are no CPs between non-adjacent atoms, but the ring center shows a CP. There is considerable similarity in the positions of the CP between the neutral and ionic states, implying very similar σ-polarization; only the 1^2B_2 state is exemplified as a result of these similarities.

The integrated intensities for the atomic basins at the unique centers are shown in the supplementary material as Table SM3. These show that the O_4 and O_1 oxygen atoms have very similar total electron densities, while their attached C-atoms, C_4 and $C_2 + C_6$, all have similar electron densities. These conclusions are distinct

TABLE I. Calculated frequencies and assignments for the X^1A_1 state of γ-pyrone compared to experimental values.

Anharmonic frequency (cm^{-1})	Harmonic frequency (cm^{-1})	Normal mode	Ascending sequence	Symmetry	Infrared (cm^{-1})[50]	Raman (cm^{-1})[50]	Fausto *et al.* HF/6-31G*[50]
3111	3246	1	27	A_1	3092	3130	3067
3128	3225	2	25	A_1	3045	3076	3038
1766	1794	3	23	A_1	1677,1659	1700,1672	1757
1685	1716	4	22	A_1	1637	1658	1656
1403	1434	5	19	A_1	1399	1398	1390
1206	1224	6	16	A_1	1203,1197	1198	1178
1014	1031	7	14	A_1	1010,1004	1008	988
938	953	8	11	A_1	922	924	907
799	820	9	8	A_1		790	769
503	509	10	5	A_1	503	504	479
982	1003	11	13	A_2			987
823	837	12	9	A_2	(824)	822	808
404	410	13	2	A_2			393
976	997	14	12	B_1	969	960	981
870	882	15	10	B_1	852	850	850
738	749	16	7	B_1	734	730	721
441	449	17	3	B_1		395	418
155	158	18	1	B_1		175	152
3111	3243	19	26	B_2	3068	3095	3064
3126	3225	20	24	B_2	3021	3076	3037
1617	1650	21	21	B_2	1610	1610	1589
1404	1446	22	20	B_2	1469,1462	1415	1399
1327	1355	23	18	B_2	1319	1318	1304
1211	1238	24	17	B_2	1216	1220	1193
1032	1052	25	15	B_2	1029,1026	1029	1013
646	653	26	6	B_2	644	641	621
461	463	27	4	B2	456	453	442

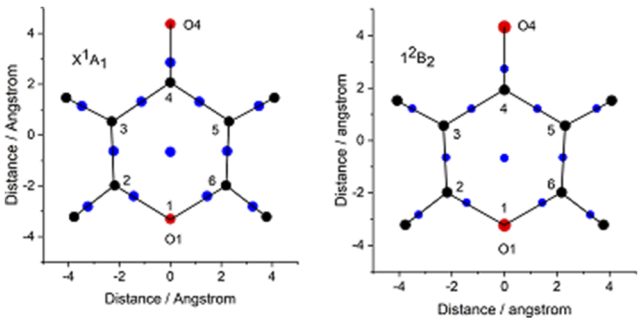

FIG. 4. The critical points (CP, marked in blue) along the bonded pairs of atoms are as determined by the Atoms in Molecules (AIM) approach. These are the positions where the electron density along the axis between a pair of atoms, as determined from the integrated electron density, reaches a minimal value. The regions between a CP and an individual atom represent the intersection of the two atomic basins. A local minimum occurs at the ring center with respect to all of the ring structure, both in the ground state and all of the ionic states at the CAM-B3LYP level. The ionic states are represented by the 1^2B_2 ionic state; the other ionic states give very similar sets of CP.

from Mulliken analyses, where the atomic populations of basis functions (BFs) are summed; in such analyses, the total density associated with a basis function (BF) is attributed to the atom where the BF is based.

B. The ionic states

General points. The principal orbitals of interest for the γ-pyrone skeleton are the π- and lone pair-molecular orbitals (MOs), shown in Fig. 5, together with the X^1A_1 ground state. The two highest occupied molecular orbitals (HOMOs, $6b_2$ and $3b_1$) have nearly degenerate orbital energies at the Hartree–Fock single configuration level; the corresponding ionic states, 1^2B_2 and 1^2B_1, are dominated by the vacancies $6b_2^{-1}$ and $3b_1^{-1}$, at the symmetry-adapted cluster configuration interaction (SAC-CI) level (Table II). The symmetric π-MOs, 1^2B_1 to 3^2B_1, show an unusual electron distribution, especially in 2^2B_1, where the C_2 + C_6 atoms are nodal. The upper part of the MO has a similar grouping to the trimethylene methane [$C(CH_2)_3$] system;[56,57] this molecule has the highest sum of bond orders in any hydrocarbon and was extensively studied by MO methods prior to its detection as a triplet state, where it was

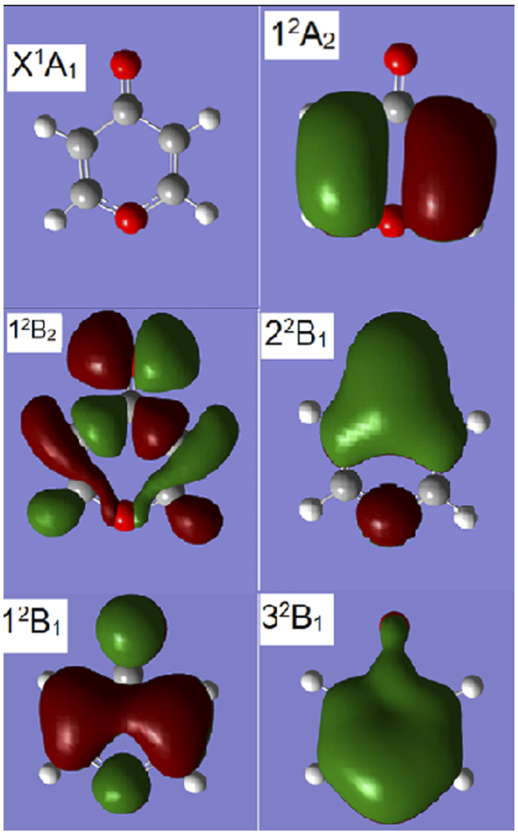

FIG. 5. The lowest π- and σ-orbital electron density contours, together with the structure of the X^1A_1 ground state, where the hatching between O_1 and $C_2 + C_6$ is a feature of the graphical drawing package, is merely diagrammatic, and shows the fully conjugated system.

identified by electron spin resonance and other methods.[58–63] The lowest γ-pyrone IE, 1^2B_2, shows a much more complex set of density nodal planes than expected for what is historically a lone pair orbital on an O_4 atom. The next IE, 1^2B_1 shows the direct interaction between the two oxygen atoms with the C=C π-bonds.

1. The wide scan photoelectron spectrum

The wide-scan PES, depicted in Fig. 2 above, also shows the SAC-CI calculated VIE and their intensities (pole strengths) superimposed; the numerical results are shown in Table II. Generally, the SAC-CI main groupings match reasonably well with the experimental spectrum over a wide energy range. In Fig. 2, the SAC-CI energies have been slightly scaled to bring the calculated ionizations in the 20–27 eV range closer to the broad peaks observed in that range of the PES; the linear correlation derived is $IE_{Observed} = 0.9198 * IE_{Calc} + 0.987$ eV; the slope close to unity and small intercept is typical of our recent studies.[1,3,5,7] Pole strengths range from zero to one; those shown in Fig. 2 have been increased by 0.05 units to make the contributions of numerous higher-energy ionic states more obvious; most of these have very low intensities. The 2^2B_1 and 1^2A_1 states are effectively degenerate in the SAC-CI study but separated by 1471 cm^{-1} (0.182 eV) in the CASSCF determination. Under similar CASSCF conditions, the 3^2B_1 and 3^2B_2 states are separated by 2383 cm^{-1} (0.296 eV). The 1^2B_2 and 3^2B_2 states are separated by 3.567 eV.

A related single-excitation configuration interaction method, the Tamm-Dancoff approximation (TDA),[41–43] also generates a very similar correlation up to 23 eV and hence is not shown. These theoretical energies enable correlation with the experimental PES; many more high-energy states are potentially exhibited by this method, and at a significantly lower computational cost.

TABLE II. The low-energy region of the photoelectron spectrum of γ-pyrone determined with the scaled symmetry-adapted cluster CI (SAC-CI) theoretical pole strength intensities. Entries are limited to pole strengths greater than 0.1; a further selection is in the supplementary material as part of SM4. In Fig. 3, the SAC-CI results have been scaled to fit the experimental energy range, using the linear correlation $IE_{Observed} = 0.9198 * IE_{Calc} + 0.987$ eV.

SAC-CI calc. IE (eV)	SAC-CI scaled IE (eV)	Intensity	Symmetry	Band assignment in Fig. 2
9.193	9.325	0.755	1^2B_2	A
9.282	9.407	0.789	1^2B_1	
−780	10.787	0.795	1^2A_2	B
13.234	13.047	0.722	2^2B_1	C
13.373	13.175	0.778	1^2A_1	
13.848	13.612	0.773	2^2B_2	D
14.563	14.271	0.744	2^2A_1	
16.015	15.608	0.727	3^2B_1	E
16.058	15.648	0.770	3^2B_2	
16.901	16.424	0.768	3^2A_1	F
17.702	17.162	0.746	4^2B_2	G
18.343	17.752	0.737	4^2A_1	
20.764	19.982	0.279	5^2A_1	H
21.064	20.258	0.382	6^2A_1	
22.222	21.324	0.463	5^2B_2	I
22.473	21.555	0.216	6^2B_2	

2. Assignment of the ionic state vibrational structure

Determination of the adiabatic ionization energies using the CAM-B3LYP functional shows that the AIE for the two lowest ionic states is reversed from the Hartree–Fock single-configuration order of VIE; the AIE are 1^2B_2 9.065 and 1^2B_1 9.328 eV. The experimental PES separation of the two IE is 0.20 eV, as discussed below. The only other low-lying AIE are 1^2A_2 and 1^2A_1, where we calculate their closeness to 11 and 13 eV, respectively.

C. Vibrational structure

1. The ionic states (1^2B_2 and 1^2B_1) in the energy range 9.2–9.9 eV (Band A)

This onset band, shown in Fig. 6, is complex and cannot be rationalized solely in terms of the predicted vibrational structure for the lowest ionic state, 1^2B_2, at the Franck–Condon level (FC). However, if the observed band is accepted as the resultant profile from both 1^2B_2 and 1^2B_1, we arrive at the combined profile shown and as listed in Tables III and IV. All the observed principal peaks are accounted for with the exception of those in the region between

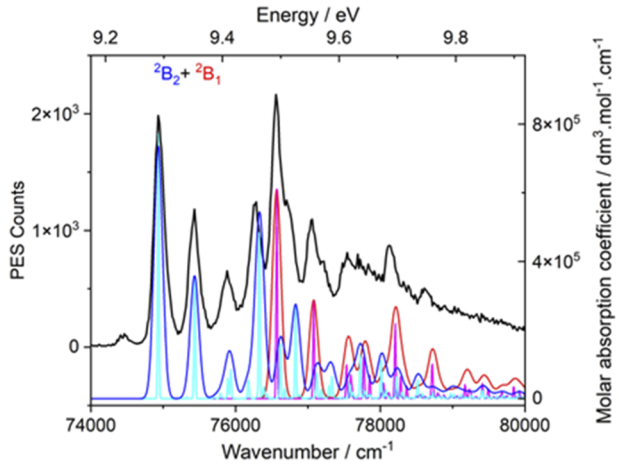

FIG. 6. The onset (Band A) of the photoelectron spectrum of γ-pyrone showing the overlap of the Franck–Condon profiles for the 1^2B_2 (in blue) and 1^2B_1 (in red) ionic states. The inset peaks have half-widths at half-maximum (HWHM) of 10 and 70 cm^{-1}.

77 500 (9.609 eV) and 78 000 cm^{-1} (9.671 eV). The calculated separation of the two states given above is 2121 cm^{-1} (0.263 eV), relatively close to the calculated separation of the 0-0 bands for the two states. These 0-0 bands are by far the most intense in either state. This analysis is limited to FC assignments and ignores Herzberg–Teller (HT) effects, where non-symmetric vibrations are allowed. Currently, we are unable to perform HT on ionic states since the Pisa version of the software has not yet been extended to ionic states. This is discussed further below.

Clearly, the vibrational profiles (VP) for these two states overlap considerably. In the case of iodobenzene, where similar overlapping VP occur for the A^2A_2 and B^2B_2 states, in order to simulate the observed spectra, different bandwidths (line widths) were required for each state.[64] The increase in the required bandwidths was attributed to internal conversion between these two states and also to the lowest state, X^2B_1, which shows a highly resolved spectrum. The study of the band separations between the four lowest IEs of the 4-mono-halogenobenzenes gave a good demonstration of the effect; bands vary in energy with change in the halogen; the reader is referred to Fig. 2 in the iodobenzene study.[64] The fluorobenzene results extend several earlier studies on the vibronic coupling

TABLE III. The onset and active fundamentals for the 1^2B_2 state, using spectroscopic sequence numbering. The energy of the 0-0 transition is 72 942 cm^{-1}, prior to a linear shift for coincidence with the PES. All intensities are given in units of molar absorption coefficient (dm^3 mol^{-1} cm^{-1}). The full list of fundamentals for the state is shown in the supplementary material as SM5.

Energy (cm^{-1})	Intensity	Spectroscopic sequence	Energy (cm^{-1})	Intensity	Spectroscopic sequence
0	515 100	0^0	1244	34 330	6^1
397	2 780	18^2	1273	1 313	$10^1 27^2$
501	208 700	10^1	1361	4 161	$9^1 10^1$
772	2 443	27^2	1396	322 500	5^1
860	10 560	9^1	1446	11 890	4^1
898	1 529	$10^1 18^2$	1464	14 280	$8^1 10^1$
962	40 000	8^1	1503	6 014	10^3
1002	56 440	10^2	1685	90 780	3^1

TABLE IV. The onset and active fundamentals for the 1^2B_1 state. All intensities are given in units of molar absorption coefficient (dm^3 mol^{-1} cm^{-1}). The full list of fundamentals for the state is shown in the supplementary material as SM6.

Energy (cm^{-1})	Intensity	Spectroscopic sequence	Energy (cm^{-1})	Intensity	Spectroscopic sequence
0	611 000	0^0	1204	119 200	6^1
371	1 234	18^2	1248	1 028	$12^1 13^1$
511	213 600	10^1	1287	50 970	5^1
681	3 359	$17^1 18^1$	1362	1 657	$15^1 17^1$
827	39	9^1	1451	16 070	4^1
965	93 340	8^1	1475	45 020	$8^1 11^1$
1021	56 490	10^2	1532	9 677	10^3
1040	21 530	7^1	1550	13 060	$7^1 10^1$
1192	1 028	$10^1 17^1 18^1$	1638	177 100	3^1

leading to conical intersections (CONINT) between the X^2B_1 and A^2A_2 states and a further trio for the B, C, and D states.[65] We note that all the main peaks of the PES onset between 9.2 and 9.8 eV are interpreted by FC vibrations; this suggests that HT factors may be small in this case, but this is discussed further below.

Returning to the present spectra, the most intense vibrational satellites for 1^2B_2 shown in Table III have a pattern that persists in the other ionic states. The types of vibrational FC modes excited for the 1^2B_1 state have similarities to those excited for the 1^2B_2 state; in both, the 0-0 bands are intense with several strong fundamentals. Sequences of the a_1 fundamentals with increasing numbers of quanta occur for all the ionic states considered. For 1^2B_2, the fundamentals 10, 9, 8, 6, 4, and 3 are present, but modes 1 and 2 (C–H stretch) do not occur. Even quanta of some of the low Herzberg–Teller (HT) modes of a_2, b_1, and b_2 symmetry also occur both here and for other ionic states considered below; a more complete analysis, including HT states, is not possible with our current software but would be expected to participate in the higher energy profile of this and other bands. A full list of harmonic frequencies for the 1^2B_2 state is shown in the supplementary material as SM5.

The principal fundamentals excited for 1^2B_1, are modes 10 down to 3, and again excluding C–H stretching modes. The second most intense peak is 10^1, and this occurs with an increasing sequence of quanta. The three lowest frequencies, all non-symmetric, namely 371 ($5b_1$), 753 ($3a_2$), and 879 ($9b_2$) cm^{-1}, occur with even numbers of quanta. The binary combination bands include several of the HT(non-symmetric) type, such as the modes at 681 cm^{-1} ($17b_1{}^1 18b_1{}^1$) and 1028 cm^{-1} ($2a_2{}^1 3a_2{}^1$). A triple combination band at low energy related to the former binary 681 cm^{-1} is at 1192 cm^{-1} ($10^1 17^1 18^1$). A full list of the harmonic frequencies in ascending frequency sequence is shown in the supplementary material as SM6.

2. Vibrational structure of the ionic state (1^2A_2) in the energy range 10.5–11.7 eV (Band B)

This IE is assigned to the 1^2A_2 ionic state and is shown with its Franck–Condon analysis in Fig. 7. This is the lowest ionic state to show an imaginary frequency (−56 cm^{-1}, $5b_2$). The full list of ascending harmonic frequencies is given in the supplementary material as SM7. The full onset up to ~1000 cm^{-1} and selected intense peaks are shown in Table V. The most prominent vibrational satellites that occur are the a_1 modes 10 down to 3; binary combinations with mode 10 are notable. All of the low-frequency non-symmetric modes, 10, 13, and 17, occur as even harmonics.

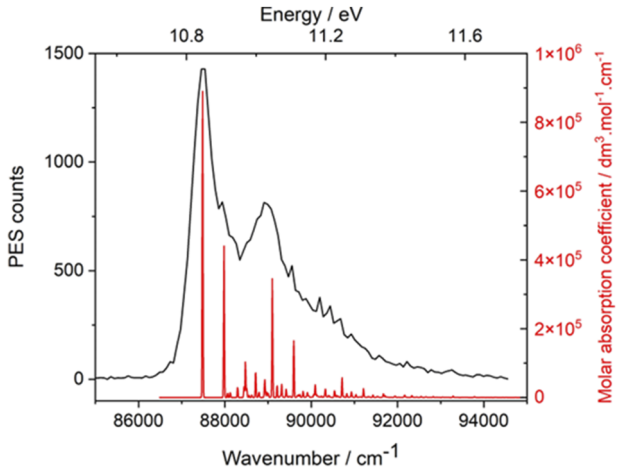

FIG. 7. Band B, the 10.5–11.7 eV range of the photoelectron spectrum, with the Franck–Condon profiles of the 1^2A_2 ionic states superimposed.

3. Vibrational structure of the ionic states in the range 12.5–14 eV (Band C)

An expanded version of this range, shown in Fig. 8, is a complex profile that seemed likely to contain three ionizations, 2^2B_1, 1^2A_1, and 2^2B_2 on the basis of the SAC-CI calculations in Table II. The relatively separated onset peaks between 12.5 and 13.0 eV are characteristic of π-ionizations and is attributed to 2^2B_1. The $^2A_1$ envelope is superimposed on the PES after amplifying its intensity by a factor of five relative to the 2^2B_1 ionic state. The CAM-B3LYP

TABLE V. The onset and active fundamentals for the 1^2A_2 state. All intensities are given in units of molar absorption coefficient ($dm^3\ mol^{-1}\ cm^{-1}$).

Energy (cm^{-1})	Intensity	Spectroscopic sequence	Energy (cm^{-1})	Intensity	Spectroscopic sequence
0	890 200	0^0	1138	7 033	$10^1 13^2$
496	440 300	10^1	1162	305	13^4
581	11 520	13^2	1229	67 110	6^1
641	14 330	17^2	1307	14 270	$9^1 10^1$
811	29 040	9^1	1439	36 500	5^1
892	154	10^2	1455	10 070	$8^1 10^1$
959	21 670	8^1	1489	15 140	10^3
968	1 533	$16^1 17^1$	1521	13 000	$7^1 10^1$
993	103 000	27^2	1616	233 000	4^1
1024	27 110	7^1	1804	3 317	$9^1 10^2$
1077	5 514	$10^1 18^2$	1833	38 020	3^1

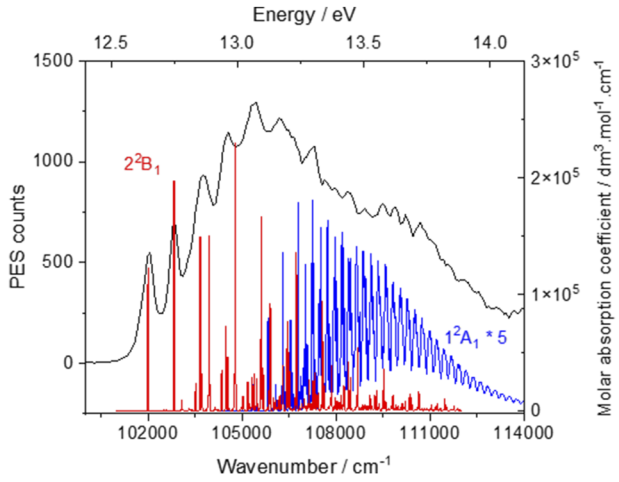

FIG. 8. Band C, the 12.5–14 eV range of the photoelectron spectrum obtained with hν = 30 eV, which leads to a resolution (ΔE = 11 meV); the Franck–Condon profiles of the 2^2B_1 and 1^2A_1 ionic states are superimposed; the much lower intensity of the latter has been amplified by a factor of 5 to make more detail apparent.

calculations (Tables VI and VII) show two of these, 2^2B_1 and 1^2A_1, differ significantly in calculated intensity. Here are several sharper (broader) peaks near 13.6 eV that do not appear to be from the other two ionizations. The structure and frequencies for 1^2A_1 were determined using the CAM-B3LYP method, as for the earlier ionic states. CASSCF studies led to (both) 2^2B_1 and 3^2B_1 states, as described in Sec. II B above.

The profiles for these two states differ significantly in character. Whereas the 0-0 band of 2^2B_1 is substantial in intensity, that of 1^2A_1 is relatively weak. Again, the vibrations present in each state are C–H deformation, out-of-plane, and ring breathing modes, with no C–H stretching modes participating in the envelope. Both profiles have the characteristic contributions from even quanta of the nonsymmetric modes; one of these for the 1^2A_1 state is of very low frequency, and this leads to the complex set of closely placed vibrations. In contrast, the 2^2B_1 state shows both much stronger and more widely spaced vibrations. The positioning of the (unscaled) theoretical set of vibrational peaks on the PES envelope is obvious for the 2^2B_1 state; the 1^2A_1 state, with its small separations, is better represented by the PES structure above 13.25 eV. The AIE for 2^2B_1 is well determined at 12.646 eV, but that for 1^2A_1 is not clear, and the positioning of it in Fig. 8 is based on the SAC-CI, discussed above, at 13.175 eV; this is not the only possible choice of energy. A full list of the harmonic frequencies for the two states in ascending frequency sequence is shown in the supplementary material as SM8 and SM9.

4. Band D with range 14.0–15.2 eV

The SAC-CI results suggest that a single 2^2A_1 state is present for this energy range. However, we have been able to determine the equilibrium structures for two states under CAS[7,8]SCF conditions, and we believe that Band D contains both the 2^2A_1 and 2^2B_2 states (Table VIII); a reasonable fit is shown in Fig. 9, but not considered in further detail.

TABLE VI. The onset and active fundamentals for the 2^2B_1 state. 0-0 transition: 98 552 cm^{-1}. All intensities are given in units of molar absorption coefficient (dm^3 mol^{-1} cm^{-1}).

Energy (cm^{-1})	Intensity	Spectroscopic sequence	Energy (cm^{-1})	Intensity	Spectroscopic sequence
0	237 900	0^0	1582	257	$7^1 10^1$
306	226	18^2	1659	180 800	9^2
510	6 093	10^1	1712	19 240	4^1
653	3 498	$17^1 18^1$	1725	295	$7^1 17^1 18^1$
830	246 000	9^1	1803	307	$6^1 10^1$
838	141	13^2	1849	67	$9^1 10^2$
860	496	$16^1 18^1$	1850	2 772	$8^1 9^1$
1019	195	10^2	1902	19 450	$7^1 9^1$
1020	2 332	8^1	1967	17 250	3^1
1072	12 800	7^1	1981	68	$9^1 26^1 27^1$
1136	200	$9^1 18^2$	2026	1 218	$5^1 10^1$
1151	43	$26^1 27^1$	2034	485	12^2
1294	4 005	6^1	2105	1 326	14^2
1339	103 800	$9^1 10^1$	2123	5 768	$6^1 9^1$
1436	550	$12^1 13^1$	2169	7 952	$9^2 10^1$
1483	5 242	$9^1 17^1 18^1$	2170	560	$5^1 17^1 18^1$
1516	27 210	5^1	2221	709	$4^1 10^1$
1553	2 253	$14^1 17^1$	2313	3 545	$9^2 17^1 18^1$

TABLE VII. The onset and active fundamentals of the 1^2A_1 state. Energy of the 0-0 transition: 101 868 cm^{-1}. All intensities are given in units of molar absorption coefficient (dm^3 mol^{-1} cm^{-1}).

Energy (cm^{-1})	Intensity	Spectroscopic sequence	Energy (cm^{-1})	Intensity	Spectroscopic sequence
0	4 512	0^0	1146	2 455	6^1
99	735	18^2	1153	1 303	$10^2 18^4$
197	161	18^4	1198	12 410	$9^1 10^1$
277	88	$17^1 18^1$	1246	4 259	$8^1 10^1$
296	57	18^6	1297	2 731	$9^1 10^1 18^1$
376	57	$17^1 18^3$	1404	12 080	$7^1 10^1$
456	112	17^2	1434	34 250	10^3
478	13 070	10^1	1440	1 825	92
555	34	$17^2 18^2$	1489	1 805	$8^1 9^1$
577	2 838	$10^1 18^2$	1503	1 686	$7^1 10^1 1^2$
720	4 542	9^1	1532	5 254	$10^3 18^2$
768	1 508	8^1	1604	1 241	4^1
926	2 915	7^1	1623	6 249	$6^1 10^1$
956	27 060	10^2	1631	1 085	$10^3 18^4$
1054	3 818	$10^2 18^2$	1646	2 717	$7^1 9^1$

TABLE VIII. The onset and active fundamentals for the 2^2B_2 state. Energy of the 0-0 transition: 111 441 cm^{-1}. All intensities are given in units of molar absorption coefficient (dm^3 mol^{-1} cm^{-1}).

Energy (cm^{-1})	Intensity	Spectroscopic sequence	Energy (cm^{-1})	Intensity	Spectroscopic sequence
0	113 300	0	1499	134 100	5^1
557	25 520	10^1	1635	31 560	4^1
1024	26 780	8^1	1931	46 460	3^1
1362	35 860	6^1	2057	44 110	$10^1 5^1$

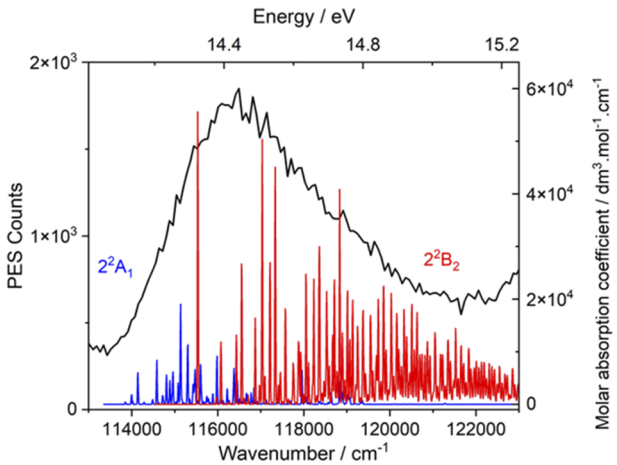

FIG. 9. Band D, the 14.0–15.2 eV range of the photoelectron spectrum obtained with hν = 30 eV, which leads to a resolution (ΔE = 11 meV). This band is thought to contain both 2^2B_2 and 2^2A_1. The two theoretical profiles have been placed arbitrarily rather than attempting an assignment.

5. Band E with range 15.1–16.2 eV

This band is shared by the 3^2B_1 and 3^2B_2 states, as shown by the SAC-CI study above. The 3^2B_2 state is dominated by the fundamental mode 9, in various combinations. The vibrational structure is superimposed on the PES for this state in Fig. 10; the onset and range up to circa 2440 cm^{-1} are shown in Table IX. However, it is clear that the a_1 fundamentals, from 10 down to 3, all occur, but with the exception of mode 9, have generally low intensity. The principal vibrational energy lies in overtones, especially mode 6, and combination bands. There are 50 vibrational state combination bands with a molar absorption coefficient $>10^4$ units (dm^3 mol^{-1} cm^{-1}), and the most intense vibration, 9472 with intensity 4580 units, is some 5857 cm^{-1} above the 0^0 band. A full list of the harmonic frequencies for the 3^2B_1 states in ascending frequency sequence is shown in the supplementary material as SM10.

6. The transition state between the 1^2B_2 and 1^2B_1 ionic states

This was performed by the combined synchronous transit and quasi-Newton methods for finding transition states (QST2 procedure) implemented in G-16.[66,67] The Cartesian coordinates for

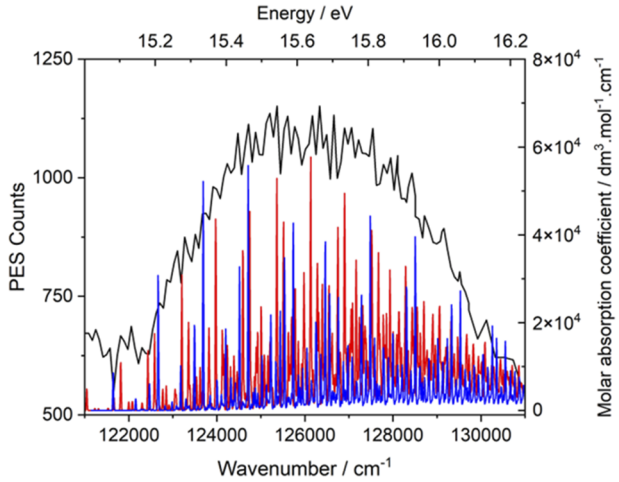

FIG. 10. Band E, the 15.1–16.2 eV range of the photoelectron spectrum obtained with hν = 30 eV, which leads to a resolution (ΔE = 11 meV). The Franck–Condon profiles of the 3^2B_1 (red) and 3^2B_2 (blue) ionic states are superimposed.

the equilibrium structures of the two states were input, using the CAM-B3LYP procedure with the 6-311G(d,p) basis set. The coordinates between the two sets of corresponding atoms are interpolated to generate a range of intermediate points. The energies of these points were determined by the same method as used for the equilibrium structures. The TS from these two states has C_S symmetry, is strongly buckled, and resembles the cyclohexane boat configuration, as shown in Fig. 11. The structure shows the necessary negative vibration frequency (−288 cm^{-1} of A' symmetry).The coordinates and the variation in bond lengths and angles between the two input

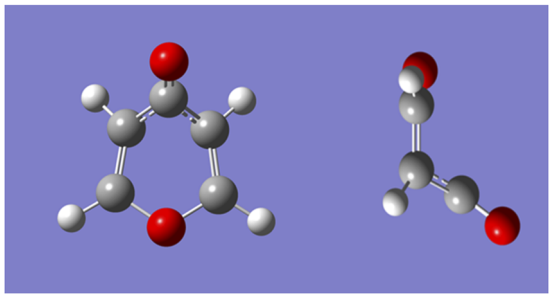

FIG. 11. The C_S symmetry transition state lying between the 1^2B_2 and 1^2B_1 ionic states is shown in two projections with similarities to the boat form of cyclohexane.

states and the TS, which are often substantial, are shown in the supplementary material as SM11.

7. Herzberg–Teller effects

As indicated above, we are currently unable to evaluate the HT vibrational coupling in cationic systems; HT calculations using the Pisa software are limited to singlet and triplet states. This is important to the present study since the calculated onset of the γ-pyrone PES shows pairs of ionic states in very close proximity, as shown in Figs. 6 and 8. It is evident that the vibrational states calculated for each state in isolation must overlap. Using the FC-calculated data, the most probable separation shown in Fig. 6 gives a reasonable interpretation of the most intense peaks observed. The Born–Oppenheimer approximation, implicit in Franck–Condon processes,[68,69] is based on the fact that the separation of electronic states is generally large compared to typical spacings associated

TABLE IX. The onset and active fundamentals for the 3^2B_1 state. Energy of the 0-0 transition: 111 441 cm^{-1}. All intensities are given in units of molar absorption coefficient (dm^3 mol^{-1} cm^{-1}).

Energy (cm^{-1})	Intensity	Spectroscopic sequence	Energy (cm^{-1})	Intensity	Spectroscopic sequence
0	1169	0^0	1906	75	8^2
476	70	10^1	1988	146	$8^1 9^1$
771	5053	9^1	2017	656	$9^2 4^1$
953	471	8^1	2029	1 199	$6^1 9^1$
1035	424	7^1	2069	65	7^2
1246	248	$9^1 10^1$	2158	11 430	$5^1 9^1$
1259	328	6^1	2200	89	$8^1 9^1 10^1$
1387	3074	5^1	2212	129	$6^1 7^1$
1533	426	4^1	2281	152	$7^1 9^1 10^1$
1541	9695	9^2	2293	108	11 14
1724	1995	$8^1 9^1$	2304	1 507	$4^1 9^1$
1799	293	3^1	2312	10 990	6^3
1805	1629	$7^1 9^1$	2315	64	$9^2 27^2$
1842	62	$9^2 17^2$	2340	1 146	$5^1 8^1$
1863	137	$5^1 10^1$	2422	961	$5^1 7^1$

with nuclear motion. When this condition is violated, residual coupling occurs via the nuclear kinetic energy operator, which causes transitions between the adiabatic electronic states.[70,71] The resultant "diabatic states" can cross, in contrast to "adiabatic states," which are subject to the non-crossing rule. We have previously shown the effect of including HT effects in some singlet states; generally, the intensities of these HT states are relatively low when compared to the 0-0 bands of the corresponding FC states. However, they do allow odd-quanta (i.e., 1-, 3-, etc.) of non-symmetric modes to participate, and that may be happening in the current ionic states.[72–75]

As stated, we cannot perform the necessary HT analysis for these ionic states. However, we have found that a transition state lies between the two separate state minima for 1^2B_2 and 1^2B_1, as described above. A conical intersection of any type necessarily causes a complete breakdown of the Born–Oppenheimer approximation,[68,69] and this provides direct evidence of the vibronic coupling between these two states.

IV. CONCLUSIONS

This study offers a new approach to the bonding of the γ-pyrone in its ground state, via the "atoms in molecules" procedure. Here, direct integration of the electron density between the constituent atoms is performed, and the boundaries of the atomic basins are defined in terms of local minima in the electron density. The σ-electron polarization is considerable. The polarity of the C–O and C=O bonds is similar, such that the observed and calculated dipole moment arises from a delicate balance between the O_1 and C_4O polarizations. Using high-order symmetry-adapted coupled cluster methods, we give a good account of the main groupings of ionization. The sequence of state adiabatic ionization energies is: $1^2B_2 < 1^2B_1 << 1^2A_2 < 1^2A_1 < 2^2B_1 <$ others, including 3^2B_1. The electron density contours of the lowest ionization (1^2B_2) show a complex structure far removed from that of the classical carbonyl group lone-pair ionization.

The first vibrational analysis of the photoelectron spectrum for γ-pyrone, enabled by a much higher resolution PES using synchrotron radiation, shows that the lowest ionization region, Band A in Figs. 2 and 6, is clearly two overlapping ionizations, 1^2B_1 and 1^2B_1. This order of states only appears at the CI level. A transition state, determined late in the investigation, between the two onset states 1^2B_2 and 1^2B_1, established that vibronic coupling between these two states does indeed happen.

All the π-electron ionizations, which lie in Bands A to E have been analyzed by Franck–Condon methods; bearing in mind the density of calculated theoretical vibrational states do not contain contributions from Herzberg–Teller processes, the envelopes are reasonably well reproduced. Even higher resolution with higher count rates would be beneficial in finalizing the experimental envelopes.

Unexpectedly, the overlap of the 1^2B_2 and 1^2B_1 ionic state vibrational envelopes does not lead to degradation of the higher-energy one. That phenomenon was observed numerous times in our studies of the halogenobenzenes previously, and the profile of the higher energy state(s) could only be interpreted by increasing the apparent vibrational line (band) width.[64,65] For example, in the case of iodobenzene, in order to simulate the observed spectra, different bandwidths are required for different states. That increase for the A^2A_2 and B^2B_2 states was attributed to internal conversion between these two states; the lowest state, X^2B_1, shows a highly resolved spectrum. The study of the band separations between the four lowest IEs of the 4-mono-halogenobenzenes gave a good demonstration of the effect; the reader is referred to Fig. 2 in the iodobenzene study.[64] The fluorobenzene results extend several earlier studies on the vibronic coupling leading to conical intersections between the X^2B_1 and A^2A_2 states and a further trio of B, C, and D states.[65] However, since the superposition of the two FC profiles gives a reasonable account of the PES, vibronic coupling is not obvious in the current cases of 1^2B_2 and 1^2B_1, where it might have been anticipated. The discovery that a transition state lies between the two equilibrium geometric ionic structures provides the necessary evidence.

SUPPLEMENTARY MATERIAL

See the supplementary material for additional information on each of the following: 1. Table SM1. Peak positions from the multi-peak analysis for the combined lowest band, assigned to the combined $^2B_2$ + $^2B_1$ and $^2A_2$ ionizations. 2. Figure SM2. The equilibrium structures of the γ-pyrone ionic states. 3.Table SM3. The integrated electron density in the atomic basins. 4. Table SM4. The higher energy region of the photoelectron spectrum of γ-pyrone determined with the scaled symmetry-adapted cluster CI (SAC-CI) theoretical pole strength intensities. 5. Table SM5. The ascending sequence of harmonic frequencies for the 1^2B_2 state with the normal mode labels. 6. Table SM6.The ascending sequence harmonic frequencies for the 1^2B_1 state with the normal mode labels. 7. Table SM7. The ascending sequence harmonic frequencies for the 1^2A_2 state with the normal mode labels. 8. Table SM8. The ascending sequence harmonic frequencies for the 2^2B_1 state with the normal mode labels. 9. Table SM9. The ascending sequence harmonic frequencies for the 1^2A_1 state with the normal mode labels. 10. Table SM10. The ascending sequence harmonic frequencies for the 3^2B_1 state with the normal mode labels. 11. Table SM11 and Fig. SM11 for the transition state lying between the 1^2B_2 and 1^2B_1 states.

ACKNOWLEDGMENTS

We thank (a) the Elettra Synchrotron facility for the grant of beamtime and C. Puglia (Uppsala University, Sweden) and the Carl Tyggers Foundation for making available the VG-Scienta SES-200 photoelectron analyzer; (b) the University of Edinburgh (Eddie3) and Edinburgh Parallel Computing Center's (Cirrus) super-computing facilities for support; (c) numerical fitting was performed using Gnuplot-5.0.5;[76] (d) plotting used Origin 7.0;[77] (e) MOs were drawn by GaussView;[78] (f) AIM densities were evaluated using AIMQB; and T. A. Keith is thanked for provision of this software.[79]

AUTHOR DECLARATIONS

Conflict of Interest

The authors have no conflicts to disclose.

Author Contributions

Michael H. Palmer: Conceptualization (equal); Methodology (equal); Supervision (equal); Writing – original draft (equal). **Marcello Coreno**: Investigation (equal); Resources (equal). **Monica de Simone**: Funding acquisition (equal); Resources (equal); Validation (equal). **Cesare Grazioli**: Data curation (equal); Investigation (equal); Resources (equal); Supervision (equal). **Nykola C. Jones**: Data curation (equal); Investigation (equal); Methodology (equal); Project administration (equal); Supervision (equal); Validation (equal). **Søren Vrønning Hoffmann**: Data curation (equal); Investigation (equal); Methodology (equal); Project administration (equal); Supervision (equal); Validation (equal). **R. Alan Aitken**: Conceptualization (equal); Methodology (equal); Resources (equal); Validation (equal). **Dheirya K. Sonecha**: Methodology (equal).

DATA AVAILABILITY

The data that support the findings of this study are available within the article and its supplementary material and also available from the corresponding authors upon reasonable request.

REFERENCES

[1] M. H. Palmer, M. Coreno, M. de Simone, C. Grazioli, S. V. Hoffmann, and N. C. Jones, J. Chem. Phys. **150**, 194305 (2019).
[2] M. H. Palmer, S. V. Hoffmann, N. C. Jones, M. Coreno, M. de Simone, and C. Grazioli, J. Chem. Phys. **151**, 084304 (2019).
[3] M. H. Palmer, R. A. Aitken, M. Coreno, M. de Simone, C. Grazioli, S. V. Hoffmann, and N. C. Jones, J. Chem. Phys. **152**, 144301 (2020).
[4] M. H. Palmer, S. V. Hoffmann, N. C. Jones, M. Coreno, M. de Simone, C. Grazioli, and R. A. Aitken, J. Chem. Phys. **153**, 054301 (2020).
[5] M. H. Palmer, M. Coreno, M. de Simone, C. Grazioli, R. A. Aitken, S. V. Hoffmann, N. C. Jones, and C. Peureux, J. Chem. Phys. **153**, 204303 (2020).
[6] M. H. Palmer, S. V. Hoffmann, N. C. Jones, M. Coreno, M. de Simone, C. Grazioli, and R. A. Aitken, J. Chem. Phys. **155**, 034308 (2021).
[7] M. H. Palmer, M. Coreno, M. de Simone, C. Grazioli, N. C. Jones, S. V. Hoffmann, and R. A. Aitken, J. Chem. Phys. **156**, 064305 (2022).
[8] M. H. Palmer, N. C. Jones, S. V. Hoffmann, R. A. Aitken, M. Coreno, M. de Simone, C. Grazioli, and I. L. J. Patterson, J. Chem. Phys. **157**, 154307 (2022).
[9] F. P. Colonna, G. Distefano, M. Guerra, and D. Jones, J. Electron Spectrosc. Relat. Phenom. **18**, 309–328 (1980).
[10] H. C. Smitherman and L. N. Ferguson, Tetrahedron **24**, 923–932 (1968).
[11] P. Beak and G. A. Carls, J. Org. Chem. **29**, 2678–2681 (1964).
[12] D. W. Mayo, P. J. Sapienza, R. C. Lord, and W. D. Phillips, J. Org. Chem. **29**, 2682–2685 (1964).
[13] C. T. Mathis and J. H. Goldstein, Spectrochim. Acta **20**, 871–878 (1964).
[14] N. M. D. Brown and P. Bladon, Spectrochim. Acta, Part A **21**, 1277–1285 (1965).
[15] R. E. Mayo and J. H. Goldstein, Spectrochim. Acta, Part A **23**, 55–60 (1967).
[16] V. Rutar and T. C. Wong, J. Magn. Reson. **53**, 495–499 (1983).
[17] C. L. Norris, R. C. Benson, P. Beak, and W. H. Flygare, J. Am. Chem. Soc. **95**, 2766–2772 (1973).
[18] R. C. Benson, C. L. Norris, W. H. Flygare, and P. Beak, J. Am. Chem. Soc. **93**, 5591–5593 (1971).
[19] J. N. MacDonald, S. A. Mackay, J. K. Tyler, A. P. Cox, and I. C. Ewart, J. Chem. Soc., Faraday Trans. 2 **77**, 79–99 (1981).
[20] G. Wlodarczak, J. Demaison, B. P. Van Eijck, M. Zhao, and J. E. Boggs, J. Chem. Phys. **94**, 6698–6707 (1991).
[21] W. H. Flygare, Chem. Rev. **74**, 653–687 (1974).
[22] D. S. Williams and T. C. Wong, J. Mol. Struct. **101**, 297–303 (1983).
[23] S. A. Spearman and J. H. Goldstein, Spectrochim. Acta, Part A **31**, 1565–1568 (1975).
[24] A. Ligabue and P. Lazzeretti, Mol. Phys. **101**, 2497–2509 (2003).
[25] C. Thomson and C. Edge, J. Mol. Struct.: THEOCHEM **121**, 173–183 (1985).
[26] E. R. Riegel and F. Zwilgmeyer, Org. Synth. **17**, 40–41 (1937).
[27] C. De Souza, Y. Hajikarimian, and P. W. Sheldrake, Synth. Commun. **22**, 755–759 (1992).
[28] M. J. Frisch, G. W. Trucks, H. B. Schlegel, G. E. Scuseria, M. A. Robb, J. R. Cheeseman, G. Scalmani, V. Barone, G. A. Petersson, H. Nakatsuji, X. Li, M. Caricato, A. V. Marenich, J. Bloino, B. G. Janesko, R. Gomperts, B. Mennucci, H. P. Hratchian, J. V. Ortiz, A. F. Izmaylov, J. L. Sonnenberg, D. Williams-Young, F. Ding, F. Lipparini, F. Egidi, J. Goings, B. Peng, A. Petrone, T. Henderson, D. Ranasinghe, V. G. Zakrzewski, J. Gao, N. Rega, G. Zheng, W. Liang, M. Hada, M. Ehara, K. Toyota, R. Fukuda, J. Hasegawa, M. Ishida, T. Nakajim, Y. Honda, O. Kitao, H. Nakai, T. Vreven, K. Throssell, J. A. Montgomery, Jr., J. E. Peralta, F. Ogliaro, M. J. Bearpark, J. J. Heyd, E. N. Brothers, K. N. Kudin, V. N. Staroverov, T. A. Keith, R. Kobayashi, J. Normand, K. Raghavachari, A. P. Rendell, J. C. Burant, S. S. Iyenga, J. Tomasi, M. Cossi, J. M. Millam, M. Klene, C. Adamo, R. Cammi, J. W. Ochterski, R. L. Martin, K. Morokuma, O. Farkas, J. B. Foresman, and D. J. Fox, Gaussian 16, Revision A. 03, Gaussian, Inc., Wallingford, CT, 2016.
[29] W. Kohn and L. J. Sham, Phys. Rev. **140**, A1133–A1138 (1965).
[30] R. G. Parr and W. Yang, *Density-Functional Theory of Atoms and Molecules* (Oxford University Press, Oxford, 1989).
[31] A. D. Becke, J. Chem. Phys. **98**, 5648–5652 (1993).
[32] T. Yanai, D. P. Tew, and N. C. Handy, Chem. Phys. Lett. **393**, 51–57 (2004).
[33] V. Barone, J. Bloino, M. Biczysko, and F. Santoro, J. Chem. Theory Comput. **5**, 540–554 (2009).
[34] J. Bloino, M. Biczysko, F. Santoro, and V. Barone, J. Chem. Theory Comput. **6**, 1256–1274 (2010).
[35] A. Baiardi, J. Bloino, and V. Barone, J. Chem. Theory Comput. **9**, 4097–4115 (2013).
[36] H. Nakatsuji and K. Hirao, Int. J. Quantum Chem. **20**, 1301–1313 (1981).
[37] H. Nakatsuji and T. Yonezawa, Chem. Phys. Lett. **87**, 426–431 (1982).
[38] H. Nakatsuji, Chem. Phys. **75**, 425–441 (1983).
[39] H. Nakatsuji, Int. J. Quantum Chem. Symp. **24**(S17), 241–255 (1983).
[40] H. Nakatsuji, K. Ohta, and T. Yonezawa, J. Phys. Chem. **87**, 3068–3074 (1983).
[41] W. von Niessen, L. S. Cederbaum, and W. P. Kraemer, J. Chem. Phys. **65**, 1378–1386 (1976).
[42] L. S. Cederbaum and W. Domcke, in *Advances in Chemical Physics*, edited by I. Prigogine and S. A. Rice (Wiley and Sons, Inc., 1977), Vol. XXXVI, pp. 205–344.
[43] W. von Neissen, J. Schirmer, and L. S. Cederbaum, Comput. Phys. Rep. **1**, 57–125 (1984).
[44] M. F. Guest, I. J. Bush, H. J. J. Van Dam, P. Sherwood, J. M. H. Thomas, J. H. Van Lenthe, R. W. A. Havenith, and J. Kendrick, Mol. Phys. **103**, 719–747 (2005).
[45] R. Ahlrichs and P. R. Taylor, J. Chim. Phys. **78**, 315–324 (1981).
[46] A. Schäfer, H. Horn, and R. Ahlrichs, J. Chem. Phys. **97**, 2571–2577 (1992).
[47] R. Krishnan, J. S. Binkley, R. Seeger, and J. A. Pople, J. Chem. Phys. **72**, 650–654 (1980).
[48] P. Császár, A. Császár, Á. Somogyi, Z. Dinya, S. Holly, M. Gál, and J. E. Boggs, Spectrochim. Acta, Part A **42**, 473–486 (1986).
[49] Á. Somogyi, P. Császár, Z. Dinya, and A. G. Császár, J. Mol. Struct.: THEOCHEM **151**, 29–37 (1987).
[50] R. Fausto, G. Quinteiro, and S. Breda, J. Mol. Struct. **598**, 287–303 (2001).
[51] V. Barone, J. Chem. Phys. **122**, 014108 (2005).
[52] R. F. W. Bader, *Atoms in Molecules: A Quantum Theory* (Clarendon Press, Oxford, UK, 1990).
[53] R. F. W. Bader, Chem. Rev. **91**, 893–928 (1991).
[54] R. F. W. Bader, "Atoms in molecules," in *Encyclopedia of Computational Chemistry*, edited by P. v. R. Schleyer *et al.* (John Wiley & Sons, Chichester, UK, 1998), Vol. 1, pp. 64–86.
[55] P. Bultinck, D. L. Cooper, and R. Ponec, J. Phys. Chem. A **114**, 8754–8763 (2010).
[56] C. A. Coulson, Discuss. Faraday Soc. **2**, 9–18 (1947).

[57] A. Streitwieser, Jr., *Molecular Orbital Theory for Organic Chemists* (John Wiley & Sons, New York, NY, 1961), Chap. 2, 2010.
[58] P. Dowd, J. Am. Chem. Soc. **88**, 2587–2589 (1966).
[59] P. Dowd and K. Sachdev, J. Am. Chem. Soc. **89**, 715–716 (1967).
[60] R. G. Doerr and P. S. Skell, J. Am. Chem. Soc. **89**, 3062–3064 (1967).
[61] P. S. Skell and R. G. Doerr, J. Am. Chem. Soc. **89**, 4688–4692 (1967).
[62] P. Dowd, Acc. Chem. Res. **5**, 242–248 (1972).
[63] Y. Yang, D. Peng, E. R. Davidson, and W. Yang, J. Phys. Chem. A **119**, 4923–4932 (2015).
[64] M. H. Palmer, T. Ridley, S. V. Hoffmann, N. C. Jones, M. Coreno, M. de Simone, C. Grazioli, M. Biczysko, and A. Baiardi, J. Chem. Phys. **142**, 134301 (2015).
[65] M. H. Palmer, T. Ridley, S. Vrønning Hoffmann, N. C. Jones, M. Coreno, M. de Simone, C. Grazioli, T. Zhang, M. Biczysko, A. Baiardi, and K. A. Peterson, J. Chem. Phys. **144**, 204305 (2016).
[66] C. Peng and H. B. Schlegel, "Combining synchronous transit and quasi-newton methods for finding transition states," Isr. J. Chem. **33**, 449–454 (1993).
[67] C. Peng, P. Y. Ayala, H. B. Schlegel, and M. J. Frisch, "Using redundant internal coordinates to optimize equilibrium geometries and transition states," J. Comput. Chem. **17**, 49–56 (1996).
[68] G. Herzberg, *Molecular Spectra and Molecular Structure. Volume III: Electronic Spectra and Electronic Structure of Polyatomic Molecules* (Van Nostrand, New York, 1966), p. 142.
[69] G. J. Small, J. Chem. Phys. **54**, 3300–3306 (1971).
[70] H. Köppel, W. Domcke, and L. S. Cederbaum, "Multimode molecular dynamics approximation beyond the Born-Oppenheimer approximation," Adv. Chem. Phys. **57**, 60–246 (1984).
[71] W. Demtröder, "Breakdown of the Born-Oppenheimer approximation, perturbations in molecular spectra," *Molecular Physics: Theoretical Principles and Experimental Methods* (Wiley, 2005), Chap. 9.
[72] W. Domcke, H. Köppel, and L. S. Cederbaum, "Spectroscopic effects of conical intersections of molecular potential energy surfaces," Mol. Phys. **43**, 851–875 (1981).
[73] A. B. Trofimov, A. D. Skitnevskaya, E. K. Grigoricheva, E. V. Gromov, and H. Köppel, J. Chem. Phys. **157**(1–16), 174309 (2022).
[74] A. B. Trofimov, D. M. P. Holland, I. Powis, R. C. Menzies, A. W. Potts, L. Karlsson, E. V. Gromov, I. L. Badsyuk, and J. Schirmer, J. Chem. Phys. **146**, 244307 (2017).
[75] A. B. Trofimov, A. D. Skitnevskaya, E. K. Grigoricheva, E. V. Gromov, and H. Köppel, J. Chem. Phys. **153**, 164307 (2020).
[76] See http://www.gnuplot.info/ for Gnuplot Release 5.0.7.
[77] Origin Version 2019, OriginLab Corporation, Northampton, MA, USA, 2019s.
[78] R. Dennington, T. A. Keith, and J. M. Millam, GaussView, Version 6.1, Semichem Inc., Shawnee Mission, KS, 2016.
[79] T. A. Keith, AIMQB (Version 14.11.23, Standard), T. K. Gristmill Software, Overland Park, KS, 2017, www.aim.tkgristmill.com.